ADVANCED FUNCTIONAL MATERIALS
www.afm-journal.de

Enhanced Resolution, Throughput, and Stability of Aerosol Jet Printing via In Line Heating

*Bella I. Guyll, Logan D. Petersen, Cary L. Pint, and Ethan B. Secor**

Aerosol jet printing offers high resolution, broad materials compatibility, and digital patterning for flexible, conformal, and hybrid electronics. However, limited throughput, instability, and complex optimization requirements inhibit translation to industrial applications. An in-line heater integrated on a custom printer is demonstrated to modulate droplet evaporation in the aerosol phase, thereby decoupling the deposition rate of functional solids and liquid ink to enable taller, narrower features with aspect ratios reaching 0.29 for a single line. Heating the printhead from room temperature to 80 °C reduced the sensitivity of resolution to deposition rate by ≈90%, improving reliability. With this strategy, increasing the linear deposition rate by 10x results in a modest increase of 27% in line width, compared to a four-fold increase without heating, permitting higher throughput without sacrificing print quality. Providing a control for in-line drying independent of ink formulation enables rapid, straightforward design of new materials and processes. This ability to engineer drying of droplets prior to impingement provides a versatile tool to meet complex fabrication challenges, as demonstrated here for both high aspect ratio printing and conformal patterning on rough and three-dimensional surfaces.

1. Introduction

Digital printing of electronic materials is an enabling capability for widespread applications in communications, healthcare, energy, aerospace, consumer electronics, and the Internet of Things.[1] Aerosol jet printing (AJP) is a non-contact, direct write technology with the versatility to support complex fabrication geometries and device functionality such as conformal antennas, sensors, electronics packaging, and hybrid flexible devices not feasible using standard methods.[2–8] AJP features micron-scale droplets (1–5 μm diameter) of functional electronic inks generated via ultrasonic or pneumatic atomization that are then transported to the printhead on a carrier gas flow.[9,10] In the printhead, an annular sheath gas accelerates the aerosol stream through a nozzle and prevents contact with interior surfaces.[11] After exiting the nozzle, droplets impinge on the target surface and coalesce into a continuous printed feature. This supports several advantages over alternative technologies including high resolution (≈10–100 μm), rapid prototyping and customization, broad material compatibility, and conformal surface deposition.[12–14] Despite its innovative approach, widespread and effective use of AJP in production settings is stymied by inherent tradeoffs in printing metrics, low material throughput, poor stability, and complex materials and process optimization.[15–18]

A prominent challenge is the tradeoff between resolution and deposition rate. While aerosol-phase focusing can be maintained to yield a well-collimated aerosol stream, deposition of excess ink on the surface can result in liquid-phase spreading. This is exacerbated at high deposition rates, for which a large volume of solvent-rich ink under a high velocity gas jet can exhibit either controlled spreading, resulting in consistently wider lines and poorer resolution, or uncontrolled wetting, resulting in irregular line edge morphology.[16] This imposes a limitation for manufacturing throughput and makes the resolution particularly sensitive to deposition rate, which is only indirectly controlled. To avoid these complications, most laboratory demonstrations throttle the deposition rate, intentionally or not, to achieve empirically better resolution, resulting in low production rates that, while tolerable in research labs, are less suitable for production environments. Additional hurdles for industrial and research applications alike include the intensive front-work associated with material and process development.[19] Even optimized inks are subject to limitations imposed by deposition rate, temperature, and geometry necessitating an acute understanding of the underlying mechanisms in order to implement appropriate operating parameters.[20–22] These challenges result in lengthened print times, prolonged ink development, aggressive platen temperatures, and sophisticated modeling to fabricate devices.

Here, we demonstrate thermal manipulation of the printhead to tailor in-line droplet evaporation. This significantly reduces the sensitivity of resolution to the deposition rate, enabling improved material throughput and stability without sacrificing high reso-

B. I. Guyll, L. D. Petersen, C. L. Pint, E. B. Secor
Department of Mechanical Engineering
Iowa State University
Ames, Iowa 50011, USA
E-mail: esecor@iastate.edu

The ORCID identification number(s) for the author(s) of this article can be found under https://doi.org/10.1002/adfm.202316426

DOI: 10.1002/adfm.202316426

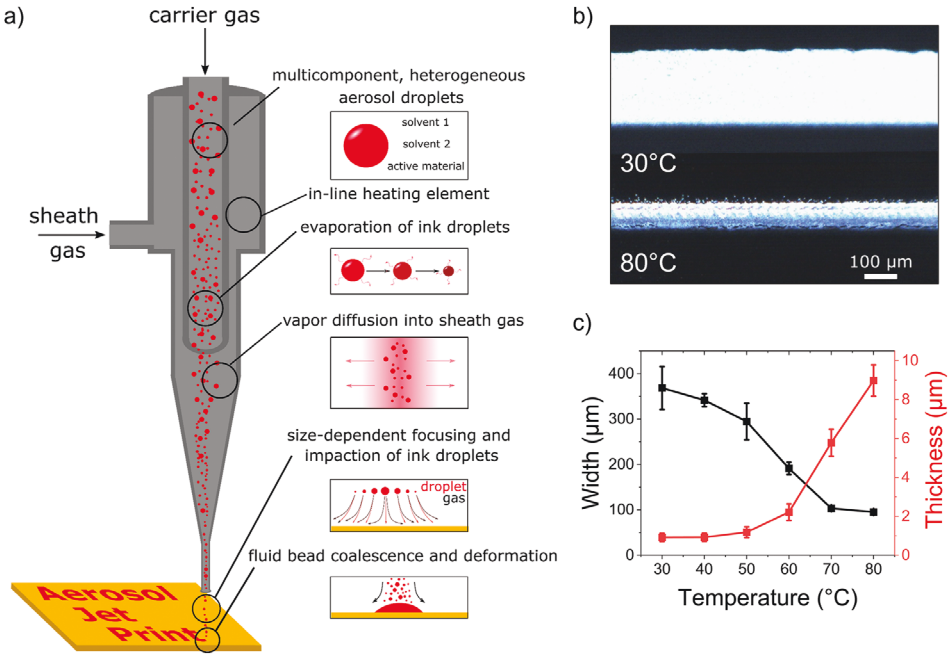

Figure 1. a) Schematic of in-line heating setup for aerosol jet printing. b) Microscope images of silver nanoparticle (AgNP) lines printed at a speed of 2 mm s^{-1} at 30 and 80 °C (top and bottom, respectively). c) Maximum thickness and line width of AgNP lines printed at a speed of 1 mm s^{-1}. Error bars represent standard deviation of n = 3 samples.

lution. This approach translates to alternative ink chemistries, a valuable capability to improve tolerance of AJP to suboptimal ink formulations and process parameters. Finally, we demonstrate its utility for printing on rough, nonplanar surfaces and in high aspect ratio, 2.5-dimensional (2.5D) architectures where traditional approaches to stabilize the process are unsuitable. In-line drying is an important mechanism for AJP, providing a useful framework to gain a fundamental understanding of droplet evaporation and to exploit it more broadly to improve the printing technology by enhancing throughput, process flexibility, and consistency.[23]

2. Results and Discussion

The typical AJP process offers operators only indirect means to modify printing deliverables. To improve the solids deposition rate, without increasing the deposition rate of liquid ink, droplet drying in the aerosol phase offers a viable mechanism (**Figure 1a**). It has been shown that in-line drying has significant implications for print quality, but the only methods to tailor this are secondary and imprecise.[20,23] For example, tuning ink volatility, aerosol volume fraction, and the focusing ratio all affect print outcomes, but also influence other characteristics and have their respective limitations. Increasing the focusing ratio, a common strategy, necessitates either a higher total gas flow rate – thus increasing nozzle pressure and susceptibility to turbulence – or a lower carrier gas flow rate (CGFR), which would directly decrease the deposition rate. This makes it difficult to overcome the tradeoff between deposition rate and resolution.

A more direct and straightforward method to decouple the solid and liquid deposition rates is to manipulate in-line evaporation. This has been mentioned in previous work, but never systematically studied to understand the process, generalize to additional materials, or address limitations.[24] Here, this is done by simply increasing the temperature of the aerosol stream and printhead during printing. Heating the aerosol is accomplished with a machined aluminum block that is in thermal contact with the flow cell and thermal isolation from the optics cell. Insertion heaters, a thermocouple, and a controller adjust the temperature of this element (Figure S8, Supporting Information).

This approach is differentiated from established thermal methods to alter printing, such as controlling platen and ink temperatures, in that it modulates aerosol droplets in flight. Higher platen temperatures can result in somewhat thinner lines by a similar mechanism, but waiting until after the ink has hit the surface to drive evaporation is less effective and limited by kinetics compared to upstream drying.[16] Moreover, heating the platen is only effective in a narrow context of printing on a thin film substrate that conducts reasonably well; for more general applications in conformal printing this cannot be universally applied. Modulating the bath temperature primarily affects the ink viscosity in the cartridge, and thus atomization and deposition rate. This has been shown to improve throughput in some cases but acts at the expense of resolution because the additional deposition of liquid would exacerbate post-deposition spreading.[25,26] Modifying droplet evaporation in flight is disparate from these processes by changing the aerosol composition prior to deposition. The short evaporation timescale and long transit time for aerosol droplets within the printhead makes them particularly sensitive to drying, allowing excess solvent to be removed prior to deposition on the surface. Moreover, because this is internal to the AJP system, it generalizes to substrates that cannot be readily heated (i.e., conformal printing or sensitive surfaces). This offers additional versatility and stability to the AJP process, broadening its manufacturing applicability.

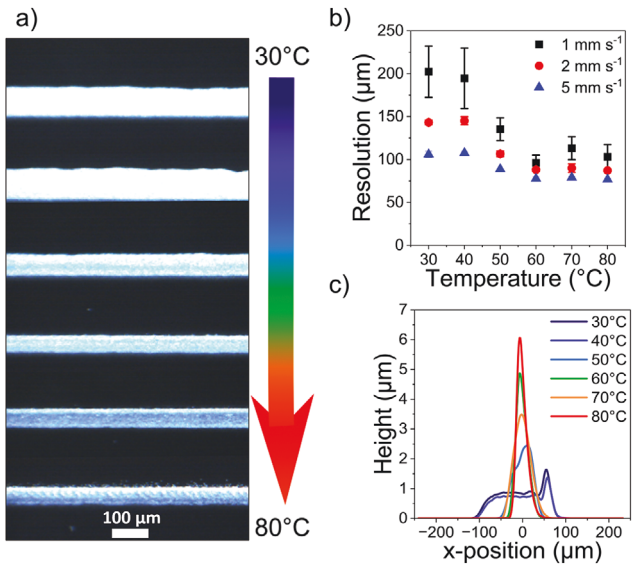

Figure 2. Effect of in-line heating on printing of AgNP ink at 12 sccm CGFR. a) Microscope images of lines printed at 2 mm $^{-1}$s for temperatures from 30–80 °C. b) Line width for print speeds of 1, 2, and 5 mm s^{-1} (n = 3 samples). c) Height profiles of lines printed at 1 mm s^{-1} for each temperature.

2.1. In-Line Heating to Facilitate Droplet Evaporation

For an initial proof of concept, a commercial silver nanoparticle (AgNP) ink was selected for its relevance to industrial applications and benchmarked printing characteristics from prior literature.[9,27] At a moderately high CGFR of 14 standard cubic centimeters per minute (sccm) and a constant focusing ratio (sheath-to-carrier gas flow rate ratio), a single printed line exhibits a wide pattern with waviness at the edges (Figure 1b, top). This is a hallmark of liquid-phase spreading following deposition, in which the low-viscosity, as-deposited ink spreads on the surface; this is based on capillarity, along with shear and pressure forces associated with the gas jet. One common approach to alleviate this is to use a faster stage speed, thus depositing less wet ink per unit length on the surface. However, this is only effective within the kinematic constraints of the motion system, and results in a thinner line as well as a narrower one. Under these same printing conditions, passing the aerosol stream through the heater at 80 °C results in much better resolution and line edge stability (Figure 1b, bottom). Put simply, while the deposition rate of solid material is the same in each case with printhead heating, the deposition rate for liquid is significantly reduced, consequently mitigating this post-impaction mechanism. Figure 1c shows the trend in both line resolution and thickness from 30–80 °C, confirming that as the line narrows the thickness increases. This improves line aspect ratios from 0.0025 to nearly 0.1 and overall consistency in line width. Above 70 °C, further heating has minimal benefit, suggesting that under these conditions the resolution is dictated primarily by where aerosol droplets impact the surface, rather than liquid-phase spreading following deposition.

To analyze this strategy in greater detail, the AgNP ink was printed at different stage speeds and temperatures with a fixed CGFR of 12 sccm and focusing ratio of 5 (**Figure 2**). As described in previous work, the speed-varying tests are an effective method to deconvolute aerosol- and liquid-phase mechanisms.[9,21] A high sensitivity of resolution to print speed is an indicator of liquid-phase spreading, which is described by a direct relationship between the resolution and speed-normalized, or linear, deposition rate under fixed gas flow conditions.[20] Figure 2b demonstrates the effect that temperature has on the AgNP ink at stage speeds of 1, 2, and 5 mm s^{-1}. Near room temperature, the resolution varies considerably between the different print speeds, but as the temperature is increased this spread is reduced. The primary transition occurs between 40–60 °C (Figure 2c), suggesting a strong vaporization of the solvents in the aerosol stream in this range. Importantly, this distinct change in printing characteristics is not accompanied by a change in electrical functionality of the printed material (Table S1, Supporting Information) or mechanical adhesion of the ink, with samples printed at 30, 50, and 80 °C all showing minimal change in resistance (<1%) during a tape peel test (Table S2, Supporting Information).

2.2. Toward High-Throughput Printing

A key benefit of in-line heating is to enable higher deposition rates without requiring a corresponding increase in print speed or line width. The effect of heating is expected to be more pronounced when liquid-phase spreading effects are exacerbated, for example at higher deposition rates. By varying the CGFR, the efficacy of in-line drying can be characterized under the higher deposition rates desired for production environments while also allowing a more quantitative analysis of experimental outcomes. **Figure 3a** illustrates the in-line evaporation effect at a CGFR of 14 sccm with the same focusing ratio and print speeds used previously (additional characterization in Figure S2, Supporting Information). At this flow rate, the effect of heating to 80 °C is more evident. By combining these two data sets and analyzing the line resolution as a function of linear deposition rate (LDR, deposition rate/print speed, equivalent to a printed line cross section area), an approximate linear relationship is observed (Figure 3b). The slope of this line, with dimensions of µm/µm^2, or µm^{-1}, is defined as the LDR sensitivity. Conceptually, this is an indicator of how sensitive line resolution is to small variations in deposition rate or print speed. It is important as a mechanism for both batch-to-batch variability and short-term fluctuations in line width, including in cases for which print speed is slightly modulated at corners to accommodate kinematic constraints of the motion system. As the printhead temperature is increased from 30 to 80 °C, the LDR sensitivity decreases from 1.14 ± 0.26 µm^{-1} to 0.13 ± 0.03 µm^{-1}, demonstrating an improvement in process reliability due to in-line heating in addition to the aforementioned improvement in throughput.

Thus far, experiments have focused on the fundamental mechanism behind in-line droplet evaporation without targeting high resolution to deconvolute the effects of droplet drying from aerodynamic phenomena. However, a key benefit of AJP in the context of digital printing methods is its high resolution capability. To demonstrate the utility of in-line heating in this process space, standard AJP practices to improve resolution (i.e., smaller nozzle diameter and higher focusing ratio) were adopted, resulting in line widths less than 30 µm (Figure 3d–f). While in-line heating

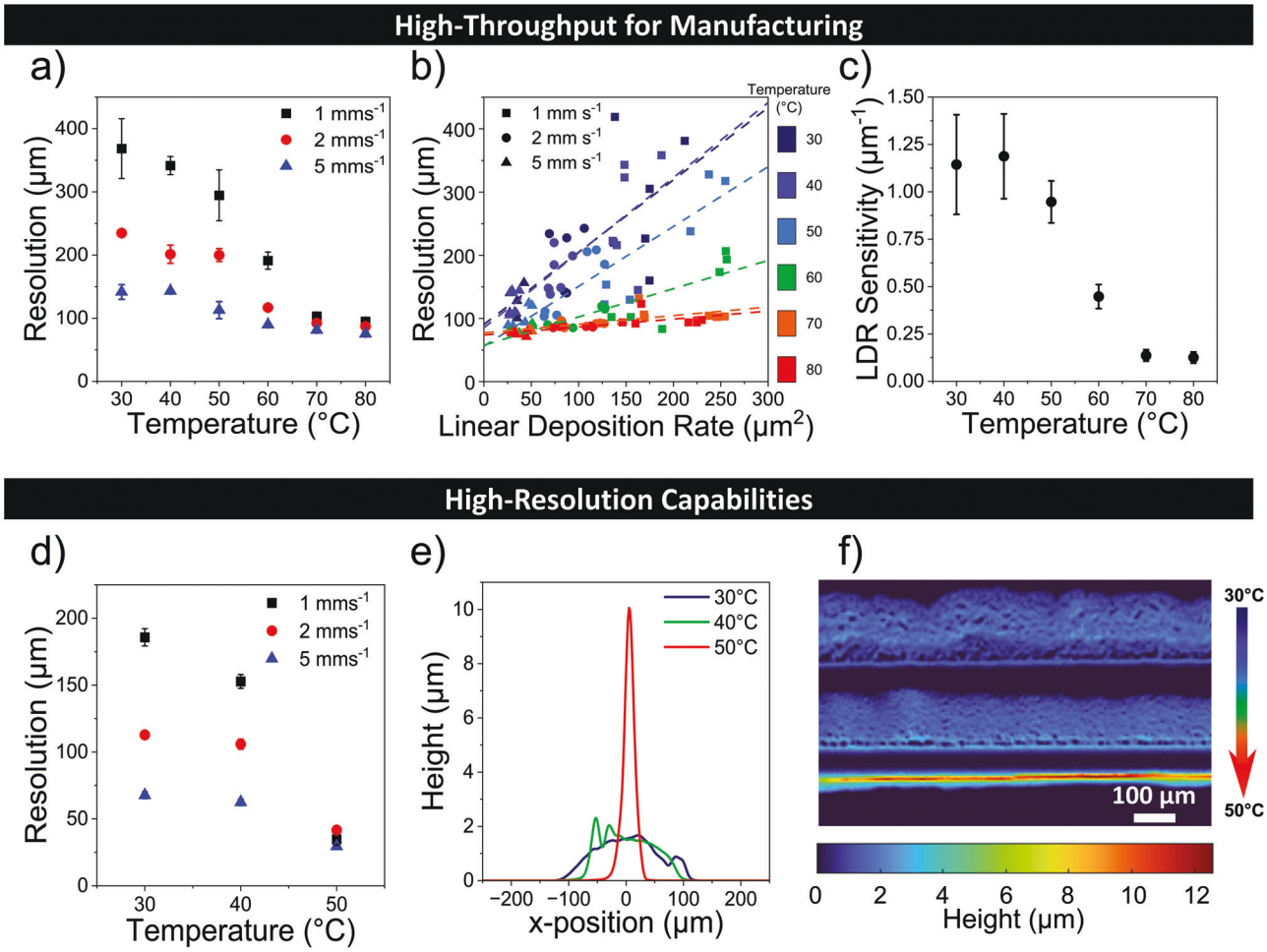

Figure 3. Utility of in-line heating to support improved manufacturing throughput (a–c) and high resolution printing (d–f). a) Width of silver lines printed at 14 sccm with print speeds of 1, 2, and 5 mm s^{-1}. b) LDR plotted against resolution for 12 sccm and 14 sccm (1, 2, and 5 mm s^{-1}) for the different temperatures. c) LDR sensitivity (ΔResolution/ΔLDR) plotted with respect to temperature (error bar represents standard error of fit). d) Line resolution for the silver ink printed with a 150 μm nozzle (14 sccm carrier gas flow, focusing ratio of 7) for print speeds of 1, 2, and 5 mm s^{-1} (average and standard deviation of 10 measurement locations). e) Height profiles for lines printed at 1 mm s^{-1} with printhead temperatures of 30 to 50 °C and f) their corresponding optical profilometry thickness maps.

alone is not viewed as a practical strategy to push the limits of AJP resolution (<10 μm), it provides a holistic improvement of the process by improving resolution without sacrificing material deposition and could reasonably support more general realization of these high resolutions with less reliance on optimization of other process parameters.

2.3. Theoretical Considerations

A better theoretical understanding of in-line evaporation can support a more rational application and generalization of this strategy. Aerosol droplets in the size range relevant to AJP are characterized by evaporation timescales on the order of milliseconds, and thus exhibit rapid evaporation until the gas phase is saturated with solvent vapor. The timescale of this process is dictated by vapor and heat diffusion in the aerosol stream, but the equilibrium towards which the system evolves is based on vapor-liquid equilibrium. Because solvent vapor pressures vary exponentially with temperature, a relatively modest adjustment to temperature can significantly alter droplet drying and, consequently, printing characteristics. This evaporation of solvent species is not a new mechanism for AJP, as it is an important process even with room temperature processing. Additional evaporation of ink droplets will slightly alter the density, and thus pressure, of the flow stream, but for typical solvents used in AJP the overall magnitude of secondary effects from this are expected to be minimal. This is because the solvent vapor in the gas phase will be limited by vapor pressure for low volatility components even at somewhat elevated temperature and by the liquid reservoir for volatile solvents, which is limited by droplet generation and transport mechanisms.

From this theoretical perspective, variables important to droplet drying within the printhead include the solvent concentrations and vapor pressures, aerosol volume fraction, focusing ratio, and temperature.[23] Although the total flow rate and internal printhead geometry influence the time evolution of the system, they are not considered in the equilibrium treatment

here. Due to the high droplet evaporation rate, it can be assumed that the carrier gas flow is saturated with solvent vapor as it exits the printer cartridge. An evolving solvent environment, initiated by changing temperature or introduction of the dry sheath gas, disrupts this equilibrium. When the sheath gas is introduced at the printhead, diffusion of the solvent vapor outward from the carrier gas drops the vapor concentration below saturation, allowing further evaporation. This results in a fairly sharp drying front moving radially inwards, which is counteracted by multicomponent solvent effects that promote more uniform drying. Inks are designed as such because complete evaporation of aerosol droplets is typically undesired, resulting in inefficient impaction, significant overspray, suboptimal microstructure, and loss of resolution.[28]

We consider the volume fraction of liquid ink in the aerosol stream as a key parameter governing liquid-phase spreading after droplets are deposited and coalesce. To estimate this, a simple calculation of the molar equilibrium considers Raoult's law (Equation 1) and mass conservation (Equation 2) for each solvent species, with the assumption of ideal mixing and ideal gas behavior:

$$\left(\frac{n_{l,i}}{\sum n_{l,i}}\right) p_{sat,i}\ (T) = n_{v,i}\ RT \tag{1}$$

$$n_{l,i} + n_{v,i} = n_{0,i} \tag{2}$$

Here, $n_{l,i}$ and $n_{v,i}$ indicate molar concentrations of component i in the liquid and vapor phase, respectively, $p_{sat,i}$ the saturation vapor pressure of the pure component i, $n_{0,i}$ the initial molar concentration of species i, R the ideal gas constant, and T the temperature.

For an n-component solvent, this results in a system of 2n nonlinear equations that can be solved with knowledge of the initial concentration and the saturation vapor pressure for a given temperature. Saturation vapor pressure is calculated using the Antoine equation for each solvent, and the initial concentration accounts for both the liquid aerosol droplets (with a given aerosol volume fraction) and the saturated carrier gas flow, assuming mole fractions equivalent to the base ink. Moreover, the initial molar concentration is scaled by the focusing ratio to reflect the introduction of dry sheath gas within the printhead. We note that this is an equilibrium, uniform calculation – it cannot reflect nonuniformity in drying across the aerosol stream or temporal effects, but nevertheless provides a useful framework to connect the effects of printhead heating, ink formulation, and printing parameters with print outcomes.

Figure S1 (Supporting Information) shows calculations of the liquid volume fraction in the aerosol stream based on this equilibrium consideration for the AgNP ink. As the temperature is increased, the liquid volume is reduced significantly, reflecting droplet evaporation. Of particular interest is the saturation in this effect when the equilibrium liquid volume approaches zero. For the AgNP ink with an aerosol volume fraction of 10^{-4}, complete drying at equilibrium is estimated at 40–50 °C. This overestimates drying since it does not incorporate nonideal mixing, solute effects on both kinetics and thermodynamics, or temporal considerations, but is in qualitative agreement with the AgNP printing results in Figures 2–3.

This mechanism by which printhead heating influences the process suggests certain limitations to its efficacy. In particular, it is explicitly intended to address the problem of liquid-phase spreading following deposition by reducing the volume deposition rate of ink (without a commensurate reduction in the solids deposition rate). In cases where print resolution is limited instead by aerosol-phase dynamics (i.e., where droplets land), heating would offer limited utility, and could exacerbate phenomena such as overspray.[29,30]

To validate this understanding, experiments were performed under drier, or solvent-depleted, printing conditions. Figure S3a (Supporting Information) illustrates that at a lower flow rate (10 sccm), with similar focusing ratios and print speeds as the previous experiments, higher resolution lines are achieved at the expense of material deposition. Smaller features can be generated at lower flow rates, but as the stream is heated the LDR drops to nearly zero (Figure S3b, Supporting Information). While this results in an apparent improvement in resolution, it is unlikely to represent optimal printing conditions in that the deposition rate is significantly suppressed. It has the effect of dried droplets either never impacting or rebounding from the surface, leading to strict requirements for ventilation and exhaust conditioning to prevent release. This is significant in that a naive attempt to optimize resolution alone will naturally push an operator into this regime of printing, despite its impracticality. To better understand where this transition occurs, the vapor saturation characteristics of the ink provide a useful guide. A crude estimate is given by the saturation ratio of the low volatility cosolvent in the aerosol stream (Equation 3).[23] Briefly, the saturation ratio compares the estimated amount of terpineol (in this case) present in the aerosol stream to the amount needed to fully saturate the sheath gas, as

$$Saturation\ Ratio\ = \frac{\upsilon_a \phi_T}{\left(\frac{p_{sat}}{RT}\right) V_m Y} \tag{3}$$

in which υ_a is the nominal volume fraction of the aerosol in the carrier gas, ϕ_T is the volume fraction of terpineol in the ink (0.1 for these experiments), p_{sat} is the saturation vapor pressure, V_m is the molar volume of terpineol, and Y is the focusing ratio. Varying temperature affects the saturation ratio most strongly via the saturation vapor pressure, which has an exponential dependence on temperature. Accordingly, increasing the temperature has a strong effect in reducing the saturation ratio. At saturation ratio values greater than 1, seen at high aerosol volume fractions (associated with increased CGFR) and low operating temperatures, cross sectional area remains relatively constant (Figure S3c, Supporting Information). At values less than 1, seen at lower flow rates and high operating temperatures (Figure S3d, Supporting Information), there is a significant depletion of material as the aerosol volume fraction decreases and the saturation vapor pressure rises. This leads to deposition rates reaching nearly zero at the highest operating temperatures. As solvent is depleted in the ink droplets, the resulting decrease in droplet diameter reduces the Stokes number, St, given by

$$St\ = C_c \frac{\rho_p d_p^2}{18\mu_f} \frac{U}{D} \tag{4}$$

in which ρ_p is the density of the droplet, d_p is the diameter, μ_f is the fluid viscosity, U is the characteristic velocity of the surrounding gas flow, D is the nozzle diameter, and C_c is the slip correction factor. A reduction in St below a threshold value causes droplets to be carried away from the printing zone on the gas flow due to their low inertia and comparative sensitivity to drag forces.[9,30,31]

These limitations highlight the importance of in-line evaporation as a means to improve throughput without sacrificing line resolution, while also revealing the potential flaws in optimization of print resolution alone. Often, efforts to achieve finer resolution in laboratory settings can inadvertently result in low deposition rates or mediocre impaction efficiency, conditions that translate poorly to production environments. By understanding and manipulating in-line evaporation, high material deposition can be achieved in tandem with resolution, with the additional benefit of reduced sensitivity to fluctuations in deposition rate.

2.4. Generalization to Other Ink Formulations

While the results thus far are based on a standard AgNP ink formulation, differences in solvent properties and ink composition will modulate the effectiveness of in-line heating. To validate the general utility of temperature manipulation, additional inks with disparate solvent chemistries are evaluated. Specifically, a conductive carbon ink (C45 carbon black) in a polar organic solvent system, along with a water-based polyimide (PI) ink, are chosen to highlight broad efficacy for nonpolar organic solvents (AgNP), polar organic solvents (C45), and aqueous (PI) formulations, along with utility for colloidal dispersions (AgNP), polymer solutions (PI), and inks containing colloids with polymer dispersants (C45) (**Figure** 4a).

Figure 4b represents the line widths associated with in-line heating of the C45 ink with constant focusing ratio and carrier gas flow rate (24 sccm; data for 20 sccm in Figure S4, Supporting Information). Data is only collected up to 50 °C because the deposition rate exhibits an abrupt drop to near-zero at higher temperatures. For this ink, height profiles corresponding to printing at 1 mm s^{-1} (Figure 4c) illustrate the main effect of in-line evaporation in the reduction of liquid phase spreading, validating applicability in a distinct, and more complex, solvent mixture. The same characteristic effect is realized for the PI ink (Figure 4d,e). Here, the aspect ratio improves up to 80 °C, showing once again that high throughput does not mandate a compromise in resolution and line edge stability.

Figure S6 (Supporting Information) shows theoretical calculations for equilibrium droplet drying corresponding to the C45 and PI solvent formulations. The C45 ink is estimated to print with a nominal aerosol volume fraction of 0.7–1 × 10^{-4}, corresponding to a saturation temperature of ≈40 °C. This corresponds reasonably well with the significant decrease in line width following printhead heating to this temperature. For the PI ink, a nominal aerosol volume fraction of 1–2 × 10^{-4} corresponds to a saturation temperature of 35–45 °C, which also coincides with the abrupt decrease in line resolution in the experimental data. This confirms that changes associated with solvent evaporation – reduced volume and increased concentration – outweigh any effects of the increased ink temperature upon deposition, which in isolation would tend to reduce viscosity and could exacerbate spreading. For the PI ink in particular, nonideal mixing and solute effects are expected to reduce drying compared to this baseline estimate. Importantly, at temperatures well above this transition, the deposition of material is maintained with reduced susceptibility to excessive drying.

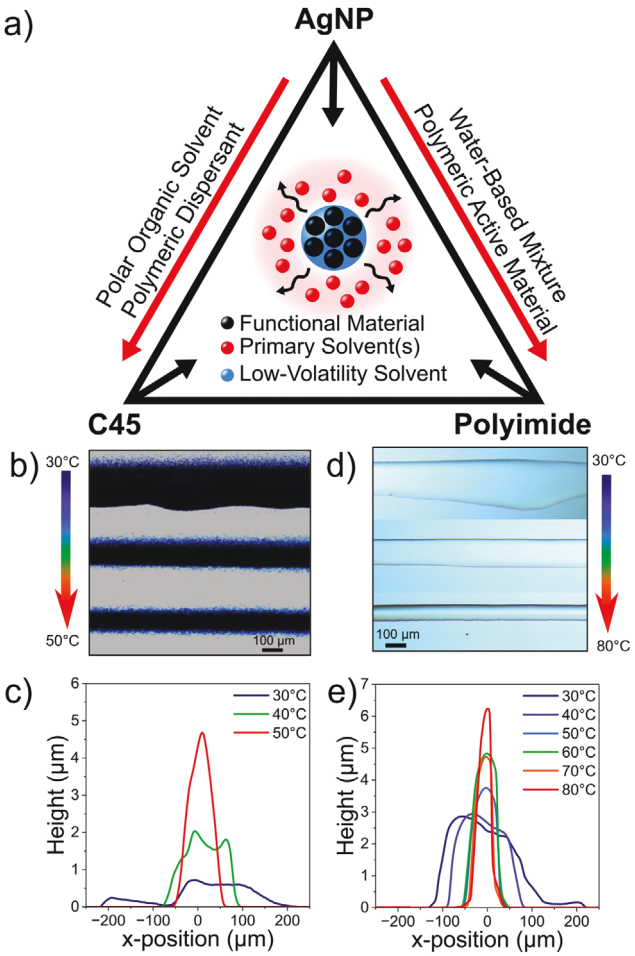

Figure 4. Generalization of in-line heating to accelerate materials development. a) Schematic illustrating droplet evaporation of the disparate AgNP, C45, and polyimide ink formulations. b) Microscope images of printed C45 lines printed between 30–50 °C. c) Height profiles of 1 mm s^{-1} C45 lines over the temperature sweep. d) Microscope images for polyimide lines printed at 30, 50, and 70 °C (additional images Figure S5, Supporting Information) and e) corresponding height profiles over the temperature sweep.

The generalizability of in-line heating to a variety of inks reveals the broader relevance beyond realizing higher deposition rates. In particular, a key strength of AJP is its suitability for rapid prototyping, an environment in which new inks and process constraints are constantly being introduced. Optimization of ink formulations is a time-consuming, Edisonian process leading to material waste. A single ink may print well at one deposition rate and temperature but have poor performance under disparate printing conditions. While optimal ink design can broaden the window of suitable printing, achieving this across different material classes is a considerable challenge. It is attractive, then, to enable a coarse optimization of ink formulation, coupled with finer

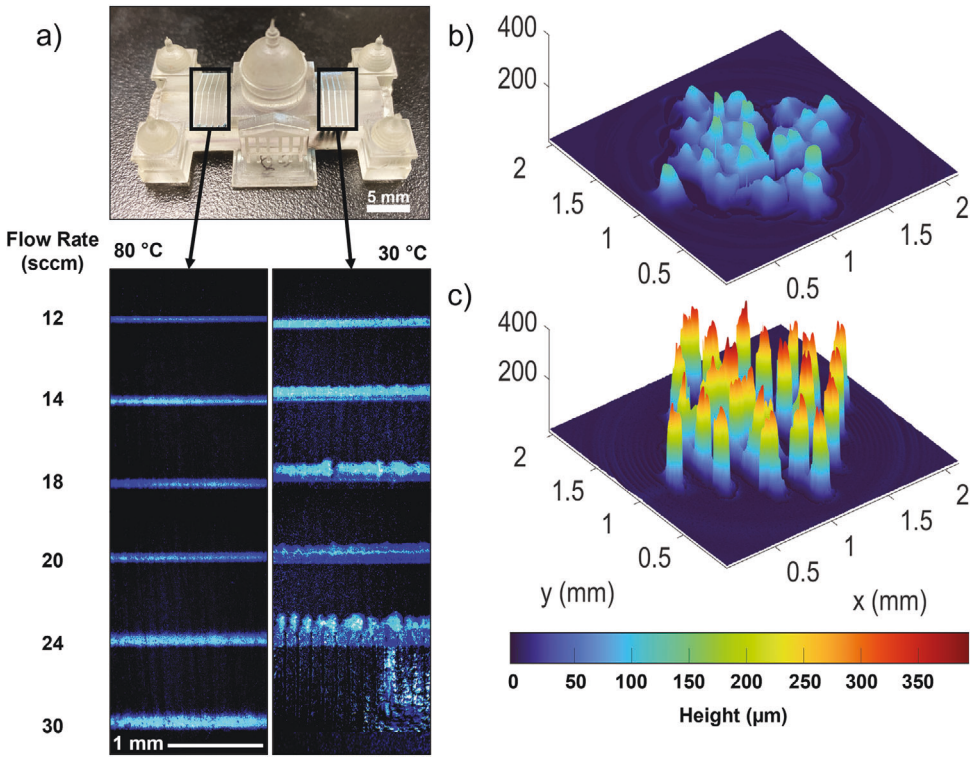

Figure 5. Conformal and high aspect ratio printing. a) Microscope images of printed AgNP lines on a conformal surface with printhead temperatures of 30 °C and 80 °C over a range of CGFRs. b,c) Optical profilometry height profiles of AgNP printed pillars at 30 and 80 °C, respectively.

tuning of the printhead temperature for efficient tailoring within more specific process requirements (i.e., different print speed limitations, throughput requirements, etc.). Having an additional lever to control the process, especially one effectively decoupled from gas flow rates and supported by theoretical grounding, is a powerful capability to broadly improve the printing process.

2.5. Conformal and High Aspect Ratio Patterning

A distinguishing characteristic of AJP is its suitability for conformal printing on complex surfaces, which is supported by non-contact, digital control with a high standoff distance.[2–5,11] In this context, conventional methods to improve print quality, such as heating the substrate, cannot be generally applied, while susceptibility to liquid-phase spreading is exacerbated in an oblique nozzle-surface orientation due to asymmetry in the gas jet. Here, in-line heating can modulate print characteristics to handle the challenges of printing on rough and nonplanar surfaces.[32] This supports electronics integration with more complex, 3D geometries and a wider scope of substrates by tailoring the ink composition and fluid properties in flight during printing.

To evaluate this, lines were patterned onto the pitched, rough surface of a stereolithography (SLA) model of the Iowa capitol. While substrate heating can sometimes help limit spreading, particularly for multilayer patterning, this would have limited efficacy on the thermally insulating SLA part with variable distance from the print surface to the heated plate. As shown in **Figure 5a**, printing at 30 °C results in irregular lines, particularly at high CGFR. When the printhead is heated to 80 °C, the line resolution and consistency is noticeably improved, with less irregular wetting due to surface roughness.

High aspect ratio printing, which implicitly leverages in-line drying and rheology changes, is another compelling capability of AJP, including a recent example of printed neural microelectrode arrays.[33,34] To demonstrate the benefit of in-line heating for high aspect ratio patterning, 2.5D pillars composed of AgNP are printed on a glass slide at 16 sccm. When printing under typical conditions with the printhead at 30 °C, the structures are ill-defined (Figure 5b). When the upstream temperature is increased to 80 °C, the deposited ink better retains the 3D shape of micropillars as high aspect ratios emerge (Figure 5c, Figure S7, Supporting Information). The ability to print each pillar continuously at high deposition rates offers unique benefits to the AJP process by limiting printing time and the need for toolpath optimization.

3. Conclusion

This work demonstrates the efficacy of in-line heating to control evaporation of droplets in the aerosol phase during AJP. This allows higher deposition rates to be used without compromising resolution, an important consideration for throughput in production environments. Moreover, in-line drying reduces the sensitivity of resolution to variations in deposition rate, improving consistency in line width. These improvements generalize to different ink compositions including silver, carbon, and polyimide, which span nonpolar organic, polar organic, and aqueous solvent

systems, along with both colloidal nanoparticles and polymer solutions, implying applicability to a broad range of water- and solvent-based inks. By adding a simple and orthogonal process control with a theoretical grounding, this capability reduces demands on formulation optimization and supports a broader window of printing parameters to better tailor deposition in different use cases. When considering more challenging printing environments, such as high aspect ratio patterning and conformal printing, which could require oblique deposition on rough and unheated surfaces, this offers a useful tool to better balance deposition and drying processes. Moreover, the magnitude and effect of deliberate in-line drying provides insight into the process mechanisms, in that droplet evaporation is important to the process regardless of whether it is explicitly controlled. Greater recognition of this during ink formulation and process parameter optimization can support more rational development. Overall, this provides a simple and effective method to better tailor AJP, with implications for throughput, consistency, fundamental process science, and process design for challenging conditions to advance applications in conformal, 2.5D, flexible, and hybrid electronics.

4. Experimental Section

Materials and Ink Preparation: Silver nanoparticle and polyimide inks were obtained from UT Dots, Inc (UTD-Ag40X and UTD-PI-SD, respectively). The conductive carbon black C45 was obtained from TIMCAL (Super C45). Solvents including isopropanol, xylenes, terpineol, dimethyl sulfoxide, isobutyl acetate, diglyme, and dihydrolevoglucosenone (referred to by its trade name, Cyrene) were purchased from Millipore Sigma and used as received. The dispersant nitrocellulose was purchased from Scientific Polymer (Cat. #712).

The silver nanoparticle ink was prepared by mixing the stock dispersion, UTD-Ag40X, with xylenes and terpineol in a 2:7:1 v/v ratio. The polyimide ink was prepared by mixing the stock solution, UTD-PI-SD, with deionized water and dimethyl sulfoxide in a 0.72:1.83:0.45 ratio. The C45 ink was prepared by mixing the raw powder (concentration 10 mg mL^{-1}) and nitrocellulose (concentration 5 mg mL^{-1}) in a solvent mixture of 2:2:1 v/v isobutyl acetate, diglyme, and Cyrene.[35] This mixture was sonicated in an ultrasonic bath overnight and probe sonicated for 10 min prior to printing.

Sample Preparation: Printing experiments were completed using a custom three axis AJP system with an ultrasonic atomizer. Light scattering measurements were taken with an optics cell to maintain consistency in atomization conditions between prints, with the optics cell thermally isolated from the in-line heater by an SLA component.[27] The in-line heater was machined from an aluminum block, with two 25 W insertion heaters (Watlow) and a k-type thermocouple connected to a PID controller (Omega Engineering). The in-line heater was configured in thermal contact with an aluminum flow cell containing the inlet for the sheath gas flow (Figure S8, Supporting Information). For printing experiments, the cartridge was actively cooled with a 20 °C water bath, the print bed was maintained at 60 °C, and the printhead temperature was controlled from 30–80 °C. Unless otherwise specified, samples were printed on glass substrates (cleaned with isopropanol) using 200 µm diameter plastic nozzles (Nordson). CGFR and sheath gas flow rate were adjusted using mass flow controllers (MFCs) while focusing ratio was held constant at 5. Following printing, silver patterns were cured on a hotplate at 250 °C for 1 hr, C45 at 350 °C for 30 min, and PI at 200 °C for 30 min using a stepped ramp (100/150/200 °C for 30 min each). A ten-pass bar was used to calculate resistances and deposition rates while additional single pass lines were printed with stage speeds of 1 mm s^{-1}, 2 mm s^{-1}, and 5 mm s^{-1} to obtain line widths and height profiles.

Characterization: Printed samples were characterized for deposition rate, resolution, and electrical resistance, where relevant. A bar containing ten overlapped printed lines (offset laterally) was used for electrical characterization and deposition rate measurements, while individual printed lines at stage speeds of 1, 2, and 5 mm s^{-1} were characterized for resolution. Microscope images for line resolution measurements were collected using an optical microscope (Motic) and analyzed for average width and standard deviation over the image length (≈3 mm) using a MATLAB script. Optical profilometry (Zygo NewView 9000) measurements were analyzed to calculate cross sectional area, thickness, and surface profiles using Gwyddion for baseline subtraction, followed by a MATLAB code. Resistance values for the silver ink were measured with a four point probe configuration using a source meter (Keithley 2450). A 10-pass bar was used for electrical measurements to reduce the error in resistivity calculations associated with the cross-sectional area values. To demonstrate mechanical adhesion, a simple tape test was implemented. Silver ink was printed at 30, 50, and 80 °C onto a plasma treated Kapton substrate. Resistance measurements were taken before and after a piece of Kapton tape was applied and removed to gauge any effect of printhead heating on ink adhesion.

Statistical Analysis: Unless otherwise specified, all data points plotted indicate the mean ± standard deviation (error bars). Line width measurements were taken as the full width at 15% of the maximum height to standardize measurements and deconvolute core line width from overspray. Cross sectional areas for resistivity calculations were average and standard deviation calculated for 10 separate regions along a total line length of 2.7 mm, and height profiles were averaged over 1.1 mm of line length. For primary experiments with the silver nanoparticle ink (Figure 1c, 2b, 3a) each data point was an average of n = 3 individual printed samples. For secondary tests (Figure 3d; Figure S4a, Supporting Information), plotted data indicate the averages and standard deviations for 10 separate segments along a total line length of 2.7 mm. Curve fitting for Figure 3b includes a data point for each individual sample (averaged over multiple measurements of a given sample), and the error bars in Figure 3c indicate the standard error of the linear fit.

Supporting Information

Supporting Information is available from the Wiley Online Library or from the author.

Acknowledgements

Funding to support this work was provided by the National Science Foundation under grant NSF CMMI-2224303. B.G. further acknowledges funding support provided by the NSF Graduate Research Fellowships Program.

Open access funding provided by the Iowa State University Library.

Conflict of Interest

The authors declare no conflict of interest.

Data Availability Statement

The data that support the findings of this study are available from the corresponding author upon reasonable request.

Keywords

additive manufacturing, hybrid electronics, multiphase flow, nanomaterial inks, printed electronics

Received: December 21, 2023
Revised: February 21, 2024
Published online: March 12, 2024

[1] Y. Khan, A. Thielens, S. Muin, J. Ting, C. Baumbauer, A. C. Arias, *Adv. Mater.* **2020**, *32*, 1905279.
[2] Y. Gu, D. Park, D. Bowen, S. Das, D. R. Hines, *Adv. Mater. Technol.* **2019**, *4*, 1800312.
[3] M. Saeidi-Javash, W. Kuang, C. Dun, Y. Zhang, *Adv. Funct. Mater.* **2019**, *29*, 1901930.
[4] S. Vella, C. Smithson, K. Halfyard, E. Shen, M. Chrétien, *Flex. Print. Electron.* **2019**, *4*, 045005.
[5] Y. Gu, D. R. Hines, V. Yun, M. Antoniak, S. Das, *Adv. Mater. Technol.* **2017**, *2*, 1700178.
[6] R. Lopez-Hallman, R. Rodriguez, Y.-T. Lai, Q. Zhang, B.-H. Tsao, J. Deiner, J. P. Fellner, Y. Zhu, *Adv. Eng. Mater.* **2024**, *26*, 2300953.
[7] M. S. Saleh, J. Li, J. Park, R. Panat, *Addit. Manuf.* **2018**, *23*, 70.
[8] C. Cao, J. B. Andrews, A. D. Franklin, *Adv. Electron. Mater.* **2017**, *3*, 1700057.
[9] E. B. Secor, *Flex. Print. Electron.* **2018**, *3*, 035002.
[10] J. A. Paulsen, M. Renn, K. Christenson, R. Plourde, in *2012 Future Instrum. Int. Workshop FIIW Proc.*, IEEE, Gatlinburg, TN, USA **2012**, pp. 1–4.
[11] T. Rahman, L. Renaud, D. Heo, M. Renn, R. Panat, *J. Micromech. Microeng.* **2015**, *25*, 107002.
[12] F. Cai, Y.-H. Chang, K. Wang, C. Zhang, B. Wang, J. Papapolymerou, *IEEE Trans. Microw. Theory Tech.* **2016**, *64*, 3208.
[13] J. Q. Feng, M. J. Renn, *J. Micro Nano-Manuf.* **2019**, *7*, 011004.
[14] W. Xie, X. Zhang, C. Leighton, C. D. Frisbie, *Adv. Electron. Mater.* **2017**, *3*, 1600369.
[15] I. S. Akhatov, J. M. Hoey, O. F. Swenson, D. L. Schulz, *J. Aerosol Sci.* **2008**, *39*, 691.
[16] M. Smith, Y. S. Choi, C. Boughey, S. Kar-Narayan, *Flex. Print. Electron.* **2017**, *2*, 015004.
[17] V. Vlnieska, E. Gilshtein, D. Kunka, J. Heier, Y. E. Romanyuk, *Polymers* **2022**, *14*, 3411.
[18] J. Wiklund, A. Karakoç, T. Palko, H. Yiğitler, K. Ruttik, R. Jäntti, J. Paltakari, *J. Manuf. Mater. Process.* **2021**, *5*, 89.
[19] H. Zhang, Z. Liu, S. Yin, H. Xu, *Sci. Rep.* **2023**, *13*, 2513.
[20] R. R. Tafoya, E. B. Secor, *Flex. Print. Electron.* **2020**, *5*, 035004.
[21] A. Mahajan, C. D. Frisbie, L. F. Francis, *ACS Appl. Mater. Interfaces* **2013**, *5*, 4856.
[22] A. Efimov, P. Arsenov, D. Kornyushin, A. Lizunova, I. Volkov, V. Ivanov, *Materials* **2020**, *13*, 730.
[23] E. B. Secor, *Flex. Print. Electron.* **2018**, *3*, 035007.
[24] C. Werner, D. Godlinski, V. Zöllmer, M. Busse, *J. Mater. Sci. Mater. Electron.* **2013**, *24*, 4367.
[25] S. Lu, J. Zheng, J. A. Cardenas, N. X. Williams, Y.-C. Lin, A. D. Franklin, *ACS Appl. Mater. Interfaces* **2020**, *12*, 43083.
[26] N. McKibben, B. Ryel, J. Manzi, F. Muramutsa, J. Daw, H. Subbaraman, D. Estrada, Z. Deng, *Microsyst. Nanoeng.* **2023**, *9*, 51.
[27] J. D. Rurup, E. B. Secor, *Adv. Eng. Mater.* **2023**, *25*, 2201919.
[28] R. R. Tafoya, E. B. Secor, *Flex. Print. Electron.* **2020**, *5*, 015009.
[29] J. Q. Feng, A. Ramm, M. J. Renn, *Flex. Print. Electron.* **2021**, *6*, 045006.
[30] G. Chen, Y. Gu, H. Tsang, D. R. Hines, S. Das, *Adv. Eng. Mater.* **2018**, *20*, 1701084.
[31] S. Ramesh, C. Mahajan, S. Gerdes, A. Gaikwad, P. Rao, D. R. Cormier, I. V. Rivero, *Addit. Manuf.* **2022**, *59*, 103090.
[32] R. Kaindl, T. Gupta, A. Blümel, S. Pei, P.-X. Hou, J. Du, C. Liu, P. Patter, K. Popovic, D. Dergez, K. Elibol, E. Schafler, J. Liu, D. Eder, D. Kieslinger, W. Ren, P. Hartmann, W. Waldhauser, B. C. Bayer, *ACS Omega* **2021**, *6*, 34301.
[33] M. S. Saleh, S. M. Ritchie, M. A. Nicholas, H. L. Gordon, C. Hu, S. Jahan, B. Yuan, R. Bezbaruah, J. W. Reddy, Z. Ahmed, M. Chamanzar, E. A. Yttri, R. P. Panat, *Sci. Adv.* **2022**, *8*, eabj4853.
[34] L. Gamba, S. Diaz-Arauzo, M. C. Hersam, E. B. Secor, *ACS Appl. Nano Mater.* **2023**, *6*, 21133.
[35] L. Gamba, Z. T. Johnson, J. Atterberg, S. Diaz-Arauzo, J. R. Downing, J. C. Claussen, M. C. Hersam, E. B. Secor, *ACS Appl. Mater. Interfaces* **2023**, *15*, 3325.